Particle Accelerators, 1992, Vol. 39, pp. 77–87
Reprints available directly from the publisher
Photocopying permitted by license only

OBSERVATION OF THE PLASMA LENS EFFECT

Y. YOSHIDA, T. UEDA, T. KOBAYASHI and K. MIYA

Nuclear Engineering Research Laboratory, The University of Tokyo, Tokai-mura, Naka-gun, Ibaraki-ken, 319-11 Japan

H. NAKANISHI, K. NAKAJIMA, H. KOBAYASHI and A. OGATA

National Laboratory for High Energy Physics, Tsukuba, 305 Japan

N. YUGAMI and Y. NISHIDA

Department of Electric and Electrical Engineering, Utsunomiya University, Utsunomiya, 321 Japan

H. SHIBATA and S. TAGAWA

Research Center for Nuclear Science and Technology, The University of Tokyo, Tokai-mura, Naka-gun, Ibaraki-ken, 319-11 Japan

(Received 19 November 1991)

A direct observation of the wakefield self-focusing of an electron beam in a plasma is reported. The transverse beam sizes were measured at three different points downstream of the plasma. The Twiss parameters and the emittance were then derived as a function of the plasma density in the overdense region. Profiles in the horizontal-longitudinal plane were also measured using a streak camera. The experimental results in the vertical direction agree well with a prediction based on linear theory.

1 INTRODUCTION

A plasma lens based on self-focusing due to the shielding of space charge of a particle beam by a quiescent plasma has been proposed as a final focus device for the next generation of linear colliders.[1] Its focusing force can exceed those of a superconducting magnet by several orders of magnitude, since a plasma can support very large electromagnetic fields. This concept is experimentally examined in this paper. The results agree well with the theoretical predictions, although certain aspects of the results remain unexplained.

There are two regions in a self-focusing plasma lens: overdense and underdense. The physical mechanism of an overdense plasma lens, in which the plasma density is much larger than the beam density, is as follows. In a relativistic electron beam traveling through a vacuum, a repulsive force caused by the space charge of all the

electrons in the bunch is canceled out by an attractive force due to the self-magnetic field of the bunch; thus, the beam almost maintains a constant radius. However, if the same beam now enters a plasma, the plasma electrons respond to the excess charge by shifting away from the beam particles. The remaining plasma ions neutralize the space-charge force within the beam; although the plasma is very effective at shielding the space charge of the beam, it is less effective at shielding its current. The beam thus experiences almost the full effect of its self-generated azimuthal magnetic field. In an underdense plasma lens, in which the beam is denser than the plasma, the space charge of the electron beam essentially blows out all of the plasma electrons, leaving a uniform column of positive ion charge.

The plasma lens effect was first demonstrated by the ANL group.[2] Because their plasma was dense and long, the focal point fell inside the plasma. They explained their results by the Bennett equilibrium. Following them, we have reported the effect of a thin overdense plasma lens[3]. The present experiments were conducted in order to verify the previous results, in which the ratio of the plasma density to the beam density was up to $n_e/n_b \sim 10$. A higher plasma density region, up to $n_e/n_b \sim 60$, was also explored in the present experiments. The results have shown that (1) the observed plasma lens effect in the vertical direction agrees well with a calculation based on linear theory;[1] (2) indication of an instability was found in the region $n_e/n_b > 50$; (3) the present results seem to reproduce the emittance reduction discovered in the previous experiments.

The experimental set-up is described in the next section. In Section 3 the results are compared with a theoretical prediction. The final section contains a discussion and conclusions.

2 EXPERIMENTAL SET-UP

The experiments were conducted at the University of Tokyo on a 18 MeV linac.[4] Figure 1 shows the experimental set-up. Single-bunch beams were introduced into a plasma chamber. Differential pumping was used to separate the plasma chamber from the linac duct. Transverse beam profiles were observed on three phosphor

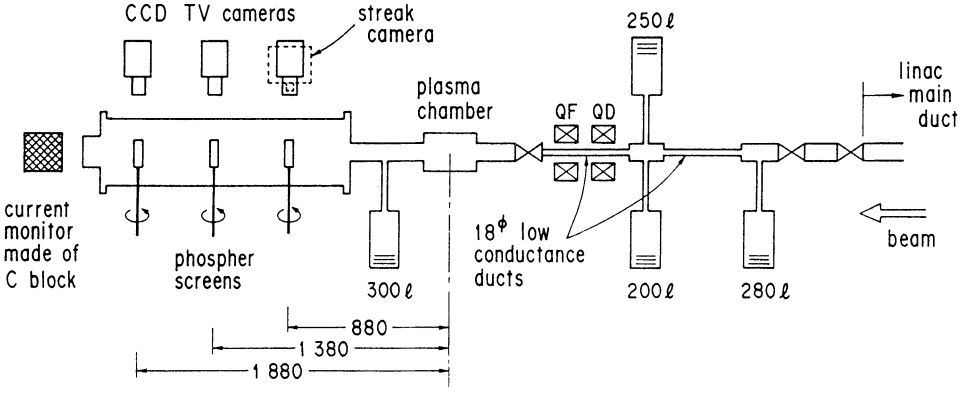

FIGURE 1 Experimental set-up. The capacities of turbomolecular pumps are given.

screens (Desmarquest AF995R) located (1) 880, (2) 1380 and (3) 1880 mm from the center of the plasma chamber. CCD TV cameras observed images on the three screens, which were triggered in synchrony with the linac beams. A carbon block was set at the end of the beamline in order to measure the beam current. The fluctuation of the current was within $\pm 5\%$ throughout the data recording. It gave the charge of a bunch as 512 pC with a repetition rate of 6.25 Hz.

The main differences from the previous experimental set-up[3] were as follows. (1) Two quadrupole magnets, a focusing-defocusing pair, were installed in front of the plasma chamber. (2) Remote control insertion and extraction of the three phosphor screens was possible, and each screen had its own CCD camera, allowing the three measurements at the three screens to be taken within one minute, before the plasma parameters changed significantly. (3) A streak camera was used to measure the beam density distribution in the horizontal-longitudinal plane.

The plasma was produced in a chamber (147 mm in inner diameter and 360 mm in length) by a discharge between the LaB_6 cathodes and the chamber in synchrony with the linac bunch. The plasma pulse width was about 2 ms. It was confined by the multidipole field of permanent magnets placed around the chamber periphery.[5] The magnetic field had its maximum value (700 G) at the chamber wall. One of the features of this confinement is that there was no magnetic field along the beam transport. The argon plasma density ranged from 0.5 to 10×10^{11} cm^{-3} and the temperature ranged from 2.5 to 4 eV, as measured by a Langmuir probe. The plasma length along the beam transport was about 15 cm.

The streak camera was placed so as to observe the same first Desmarquest screen that was used for the transverse profile measurement. The horizontal slit in front of the lens only introduced light into the camera from the vertical center of the beam. The camera caught the ultra-short decay component of the phosphorescence from the Desmarquest screen. The phosphorescent mechanism will be reported elsewhere.[6] In order to obtain good statistics in spite of the poor light intensity, we took 512 streak pictures before computer image processing.

The beam parameters at the plasma center in the absense of a plasma were as follows: $\sigma_{y0} = 2.26$ mm, $\sigma'_{y0} = 0.837$ mrad, $\rho_{y0} = -0.713$, $\sigma_{x0} = 2.77$ mm, $\sigma'_{x0} = 2.25$ mrad, and $\rho_{x0} = -0.956$. Their derivations will be described in Section 3. The streak camera measurement gave the rms bunch length as $\sigma_{l0} = 4.18$ mm; this, however, is a value calculated from a superposition of 512 streak pictures. We, therefore, used the value for a single bunch measurement obtained several years ago, $\sigma_{l0} = 3$ mm.[4] The average electron density inside the bunch becomes $n_b = 1.23 \times 10^{10}$ cm^{-3}.

These two measurements using a streak camera give the resolution of the camera in the longitudinal length measurements as $[(4.18 \text{ mm})^2 - (3 \text{ mm})^2]^{1/2} = 2.91$ mm. This must be mainly due to the time jitter of the camera triggering.

3 EXPERIMENTAL RESULTS

Figure 2 shows the typical transverse profiles on the three screens, taken by the CCD cameras and contoured by a computer. As the plasma density increases, the image

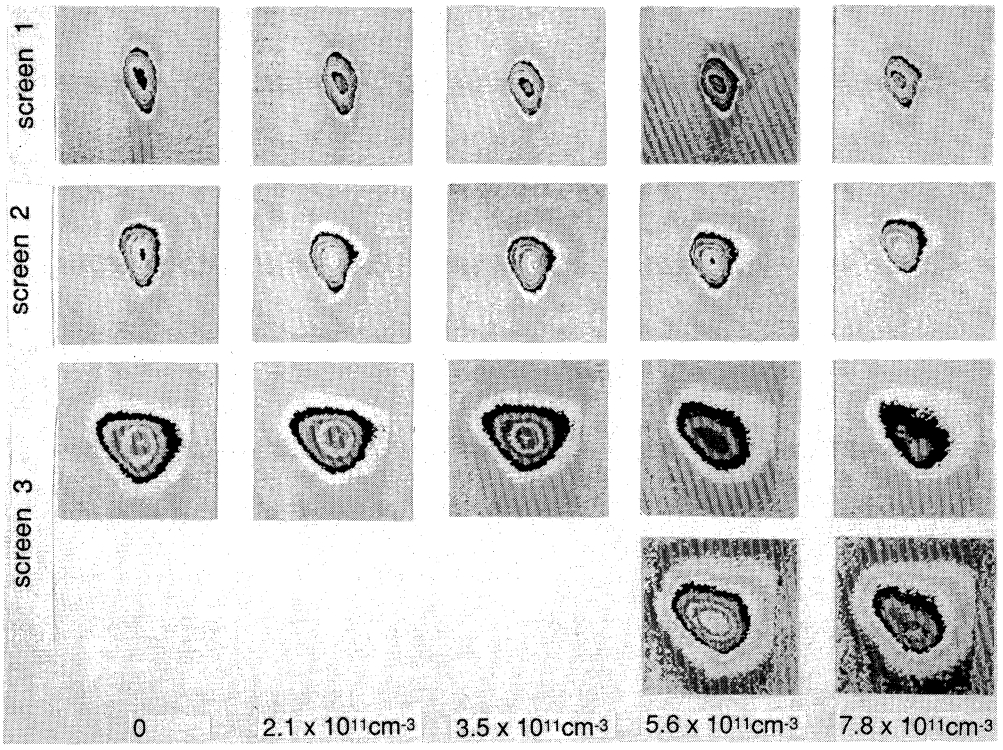

FIGURE 2 Typical transverse profiles obtained at three screens. The magnifications are different for the three screens. The contours were processed by the same rule, except for the two out of the matrix, where the sensitivity is increased.

changes mainly in the vertical direction. In the density region above 5×10^{11} cm^{-3} or $n_e/n_b > 40$, profiles contoured with increased sensitivity are also given, since the image on the third screen becomes weak and broad. Above 7×10^{11} cm^{-3} or $n_e/n_b > 50$, two peaks are distinguishable on the third screen.

The intensity distribution on each screen was integrated both vertically and horizontally. The horizontal and vertical beam sizes were calculated from the resultant one-dimensional distribution. The so-called rms beam sizes were derived from the width of the distribution, to give $\exp(-\frac{1}{2})$ of the peak. Figure 3 shows the horizontal and vertical beam sizes as a function of the plasma density. The three bold lines show an approximation using third-order (Figure 3a) and second-order (Figure 3b) polynominals. Since no remarkable change is found in the horizontal size except for in the high-density region, the following analysis is made only on the vertical size.

Because free space existed between the plasma and the phosphor screens, we could derive three parameters (two Twiss parameters and the emittance) of the plasma as a function of the plasma density from three sets of data at the screens. Let us approximate the transverse profile of the beam at the plasma position by a Gaussian characterized by three parameters, σ, σ' and ρ. Specifically, the beam in the transverse

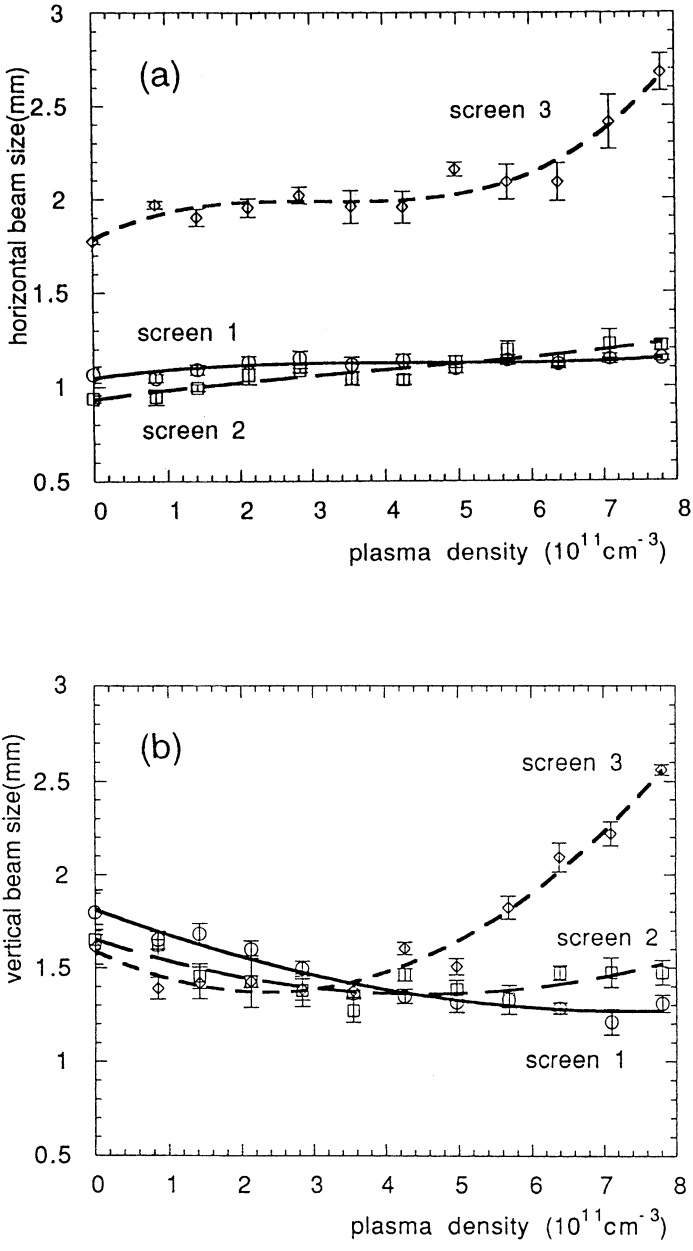

FIGURE 3 Horizontal (a) and vertical (b) beam size observed on three screens. The lines show approximations using third-order (a) and second-order (b) polynominals.

phase space at the plasma is expressed by the matrix

$$\Sigma = \begin{pmatrix} \sigma^2 & \rho\sigma\sigma' \\ \rho\sigma\sigma' & \sigma'^2 \end{pmatrix}, \tag{3.1}$$

or the contour equation of the beam is written as

$$\frac{1}{1-\rho^2}\left(\frac{y^2}{\sigma^2} - \frac{2\rho yy'}{\sigma\sigma'} + \frac{y'^2}{\sigma'^2}\right) = 1. \tag{3.2}$$

The beam at the screen i (where $i = 1, 2, 3$) is then expressed by the matrix

$$\Sigma_i = F_i \, \Sigma \, F_i', \tag{3.3}$$

where F_i is the transfer matrix of free space with a distance s_i between the plasma and the i-th screen:

$$F_i = \begin{pmatrix} 1 & s_i \\ 0 & 1 \end{pmatrix}; \tag{3.4}$$

F_i' denotes the transpose of F_i. Beam sizes σ_1, σ_2 and σ_3 at the three screens then become

$$\sigma_i^2 = \sigma^2 + 2s_i\rho\sigma\sigma' + s_i^2\sigma'^2. \tag{3.5}$$

Solving the three simultaneous equations with $i = 1, 2, 3$, we obtain σ, σ' and ρ. The Twiss parameters (β and γ) and the emittance (ε) are derived from the relations

$$\beta = \sigma^2/\varepsilon, \; \gamma = \sigma'^2/\varepsilon \quad \text{and} \quad \varepsilon = \sigma\sigma'(1-\rho)^{1/2}. \tag{3.6}$$

The vertical Twiss parameters and the emittance were calculated by two methods from the experimental data. First they were calculated directly from a trio of data: σ_1, σ_2 and σ_3. The results are plotted in Figure 4, whose dependence on the plasma density was approximated by the third-order polynomials (shown by narrow solid lines). The second calculation used a method described in a previous report,[3] in which the density dependences of the beam sizes were first approximated by quadratic curves, as shown in Figure 3(b). The Twiss parameters and the emittance were then calculated as continuous functions of the plasma density from the approximated, but continuous, beam sizes. The thick solid lines in Figure 4 show the results.

The density dependence will now be explained theoretically. In the range $n_e > 0.5 \times 10^{11}\ \text{cm}^{-3}$, Chen's conditions for the round-beam-limit, $1/(4\pi r_e a^2) \gg n_e \gg 4Nk_p^2 b/(\pi a^2)$, are satisfied,[1] where the parabolic profiles in both the transverse and longitudinal directions are assumed to be approximations to a Gaussian, with a and b denoting the bunch radius and half of the bunch length, respectively; i.e., the transver distribution is approximated by $f(r) = 1 - r^2/a^2$, and the longitudinal distribution is approximated by

$$g(\zeta) = 1 - (\zeta + b)^2/b^2, \tag{3.7}$$

where $\zeta(-2b < \zeta < 0)$ denotes the longitudinal position inside a bunch. What we observed is the rms size. The parameters characterizing the parabola distribution (a

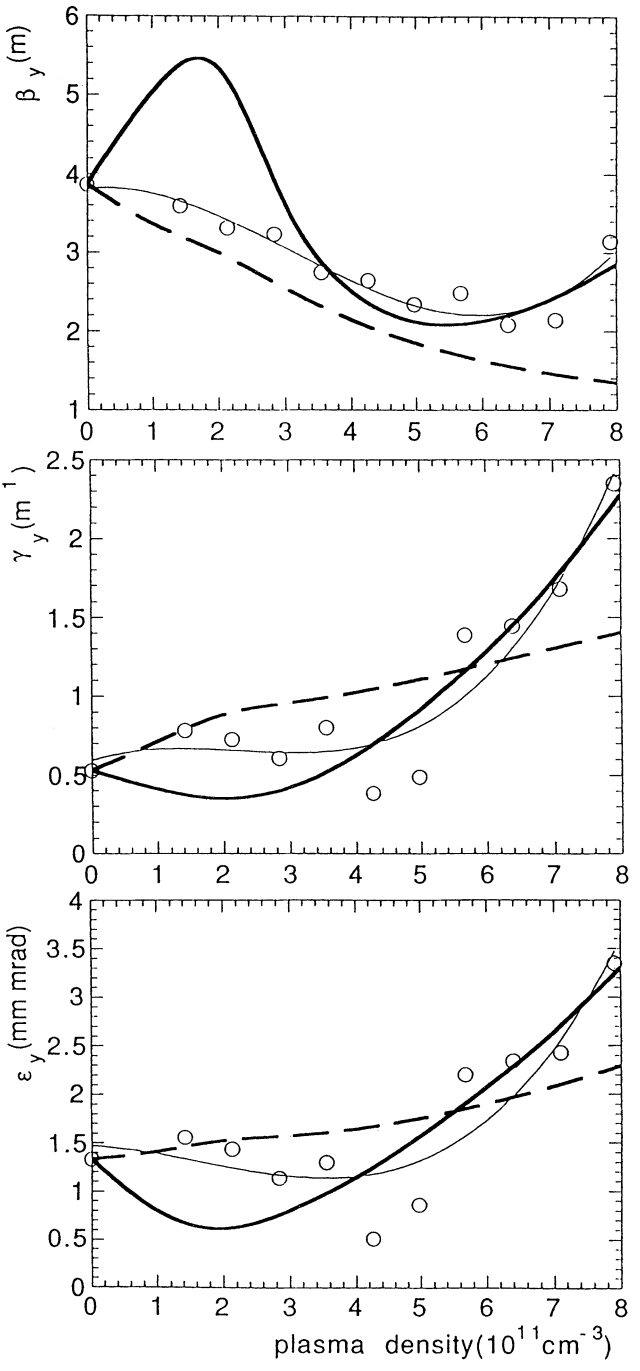

FIGURE 4 Dependence of vertical Twiss parameters and emittance on the plasma density. The data points and the thin solid lines were calculated directly from the measured beam sizes, while the thick solid lines were calculated from the quadratic approximation given in Figure 3. The dashed lines were calculated based on a round-beam model.

and b) should be determined so as to give the same area as a Gaussian distribution with the same peak intensity. This gives

$$a = (9\pi/8)^{1/2}\sigma,\ b = (9\pi/8)^{1/2}\sigma_l. \tag{3.8}$$

Under these conditions, the focusing strength is proportional to ζ^3:

$$K(\zeta) = \frac{e^2 k_p^2 N \zeta^3}{\gamma m c^2 a^2 b^2}. \tag{3.9}$$

The beam at the plasma position in the absence of a plasma can be expressed by a matrix, Σ_0. Using the familiar transfer matrix of a thick lens with length l,

$$P(\zeta) = \begin{pmatrix} \cos\sqrt{K(\zeta)}l & (\sin\sqrt{K(\zeta)}l/\sqrt{K(\zeta)} \\ -\sqrt{K(\zeta)}\sin\sqrt{K(\zeta)}l & \cos\sqrt{K(\zeta)}l \end{pmatrix}, \tag{3.10}$$

the beam in the presence of a plasma can be expressed by

$$\Sigma\,(\zeta) = P(\zeta)\,\Sigma_0\,P'(\zeta). \tag{3.11}$$

By inserting $\Sigma(\zeta)$ into Eq. (3.3), the beam parameters at a screen are obtained. Here, the result is written as $\Sigma_i(\zeta)$, because it is a function of ζ. The beam size at a screen, $\sigma_i(\zeta)$, is the square root of the (1, 1) element of $\Sigma_i(\zeta)$. The beam size that we have observed is the average of $\sigma_i(\zeta)$ weighted by the longitudinal distribution of Eq. (3.7); i.e.

$$(\sigma_0)_i = \int_{-2b}^{0} g(\zeta)\sigma_i(\zeta)d\zeta \Big/ \int_{-2b}^{0} g(\zeta)d\zeta. \tag{3.12}$$

The thick lines in Figure 5 give the theoretical density dependences of the vertical sizes at the three screens, where the lens length was set at 15 cm. As shown, the experimental and theoretical sizes agree fairly well.

Because of the nonlinear operation of Eq. (3.12), the resultant longitudinal distribution is no longer Gaussian. This operation does not conserve the emittance, but deteriorates it, if it is perfunctorily calculated from the left-hand side of Eq. (3.12), using Eq. (3.6). The dashed lines in Figure 4 show the apparent dependence of the emittance on the plasma density, together with those of the Twiss parameters, β and γ. The figure shows that the experimental emittance reduction overcomes the apparent emittance increase in the low-density region, though the density dependences of the experimentally obtained emittance are somewhat different due to the two methods of data processing.

Longitudinal profiles along the beam center were derived from the streak pictures. The longitudinal bunch sizes, the barycenter shifts and the peak intensities were then calculated. Here, the bunch size was again defined by using the full-width-exp($-\frac{1}{2}$)-maximum. Figure 6 shows them together with narrow lines approximating their density dependence by third-order polynomials. The longitudinal line distribution

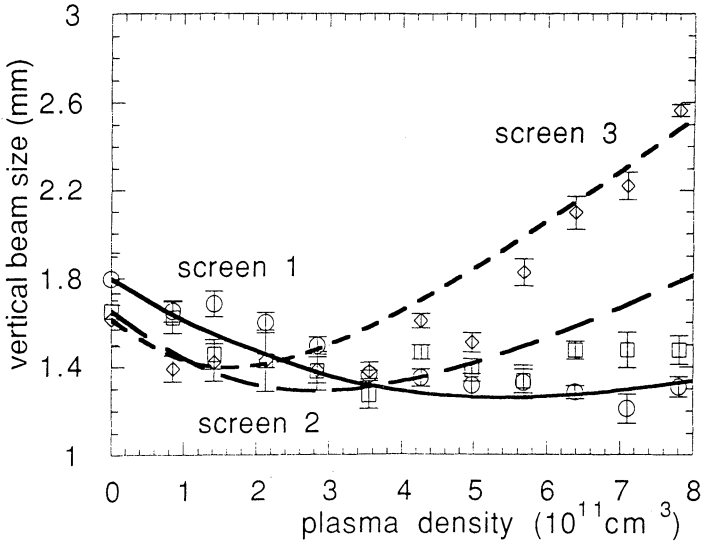

FIGURE 5 Theoretical dependences of the vertical beam sizes at three screens on the plasma density. Experimental data are also given.

should be proportional to

$$h_1(\zeta) = \frac{g(\zeta)}{\sigma_{x1}(\zeta)\sigma_{y1}(\zeta)} = \frac{1 - (\zeta + b)^2/b^2}{\sigma_{x1}(\zeta)\sigma_{y1}(\zeta)}. \tag{3.13}$$

The thick lines in Figure 6 show the width, the peak position, and the peak intensity calculated from this equation. The peak intensities were normalized by the value in the absence of a plasma. Only the plasma density dependence of the vertical size $[\sigma_{y1}(\zeta)]$ was taken into account in the calculation, while the horizontal size $[\sigma_{x1}(\zeta)]$ was regarded as constant. The finite resolution of the streak camera was taken into account in deriving both the width and the peak intensity. Though the tendency agrees between the experiments and theory, the experiments show weaker density dependences for all three curves. It should be noted that the theoretical calculation is not strict, since it adopted a parabolic distribution as an approximation of a normal Gaussian distribution.

4 DISCUSSION AND CONCLUSIONS

A comment should be made concerning the peak split appearing on the third screen at the high plasma density region of Figure 2. We found that this structure was quite robust and reproducible. It might contribute to the emittance increase at the high-density region shown in Figure 4. One of the possible mechanisms causing this peak split could be the Webel instability.[7] However, this instability is only possible for wide beams where $k_p a > \pi$. Our plasma was not sufficiently dense to fulfill this condition.

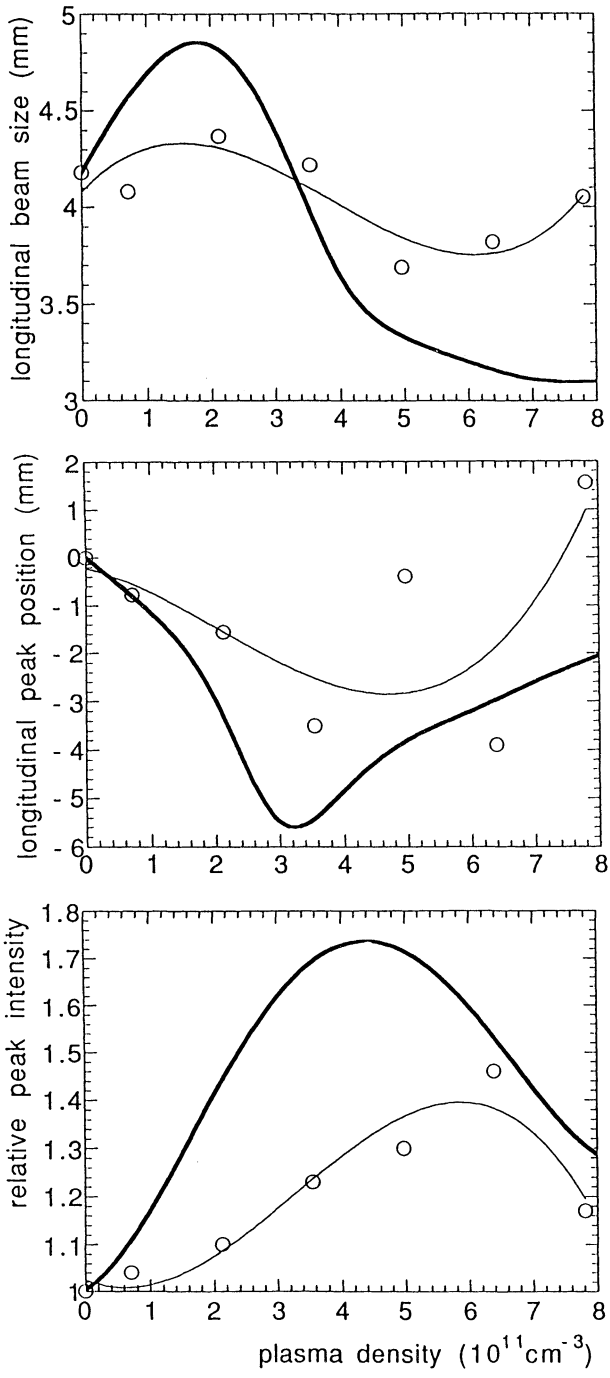

FIGURE 6 Dependence of the longitudinal bunch size, longitudinal peak position and peak intensity on the plasma density measured by a streak camera. The peak intensity was normalized by the value in the absence of a plasma. The thick solid lines show theoretical values based on a round beam model, while the thin lines show approximations of experimental data using third-order polynominals.

The phenomenon shown in Figure 3(a), the plasma lens having little effect in the horizontal direction, cannot be explained. Figure 2 shows that the vertical distribution was always broader than the horizontal distribution. This is most remarkable at the first screen. One possibility is the existence of an obstacle upstream of the plasma. If it scraped both the right and left sides of the beam, the beam could not have a Gaussian distribution in (x, x') phase space when entering the plasma. In this case, the lens could not be effective horizontally.

Figure 4 suggests the possibility that the emittance calculation adopted previously[3] might exaggerate its dependence on the plasma density. However, the same figure still shows the existence of a modest emittance decrease in the density region $n_e/n_b < 40$. A previous report[3] suggested the possibility that the decrease in transverse emittance is compensated for by an increase in longitudinal emittance. The hypothesis is as follows. The beam particles experience not only a transverse wakefield causing the lens effect, but also a longitudinal wakefield causing deceleration. It is null at the head of the beam and maximum at the tail. A substantial energy spread is thus introduced which increases the longitudinal emittance. This increase in turn decreases the transverse emittance. Although this hypothesis is plausible, no specific mechanism has yet been designated which mixes the particles in six-dimensional phase space to enable transverse-longitudinal coupling. In addition, a fact opposing this hypothesis is suggested in the present experiments: that is, the bunch length shortening shown in Figure 4. The energy spread could be compensated for by the bunch shortening so that the longitudinal emittance would be conserved independently of the transverse emittance.

The underdense region was also studied. Only a large statistical variance in the experimental data because of a weak lens effect was found. A longer plasma is necessary to study this region using this linac.

In conclusion, these experiments have verified the previous results in one aspect. The two-dimensional linear theory of plasma wakefield still explains the results, in spite of the fact that the measurement was also made in the high plasma density region of $n_e/n_b \gg 10$. However, a new phenomenon was found which caused two peaks on the transverse profile and an emittance increase in the density region above $n_e/n_b > 50$. An emittance reduction was observed below $n_e/n_b < 40$. Its mechanism still remains to be analyzed.

REFERENCES

1. P. Chen, *Part. Accel.* **20**, 171 (1987).
2. J. B. Rosenzweig, R. Schessow, B. Cole, C. Ho, W. Gai, R. Konecny, S. Mtingwa, J. Norem, M. Rosing and J. Simpson, *Phys. Fluids B* **2**, 1376 (1990).
3. H. Nakanishi, Y. Yoshida, T. Ueda, T. Kozawa, H. Shibata, K. Nakajima, T. Kurihara, N. Yugami, Y. Nishida, T. Kobayashi, A. Enomoto, T. Oogoe, H. Kobayashi, B. S. Newberger, S. Tagawa, K. Miya and A. Ogata, *Phys. Rev. Lett.* **66**, 1870 (1990).
4. H. Kobayashi, T. Ueda, T. Kobayashi, S. Tagawa and Y. Tabata, *Nucl. Instr. and Meth. B* **10/11**, 1004 (1985).
5. K. Nakajima, A. Enomoto, H. Kobayashi, H. Nakanishi, Y. Nishida, A. Ogata, S. Ohsawa, T. Oogoe, T. Shoji and T. Urano, *Nucl. Instr. and Meth. A* **292**, 12 (1990).
6. S. Tagawa, *Proc. 7th. Symp. Accel. Sci. Tech.*, Wako, Japan, 1991, p. 293.
7. J. J. Su, T. Katsouleas, J. M. Dawson, P. Chen, M. Jones and R. Keinigs, *IEEE Trans. Plasma Sci.* **PS-15**, 192 (1987).